Electronic Supplementary Material (ESI) for ChemComm.

Supplementary Information

Superior electrochemical performance of N-doped nanocrystalline FeF_3/C with single-step solid-state process

Jangwook Lee [a] *and Byoungwoo Kang*[*a]

[a] Department of Materials Science and Engineering, Pohang University of Science and Technology (POSTECH), Pohang 790-784, Republic of Korea

*Corresponding Author E-mail: E-mail: bwkang@postech.ac.kr

Experimental Section

Synthesis

Three types of FeF_3 were synthesized: ‘regular’ FeF_3 (FeF_3(R)), and two forms to which melamine had been added to provide N: FeF_3(M20) and FeF_3(M50). To synthesize FeF_3(R), PTFE (Sigma-Aldrich) and $Fe(C_2O_4)\cdot 2H_2O$ (iron oxalate, Alfa) were mixed in a ratio of 2: 1 (wt%),[1] then ball-milled overnight. To synthesize FeF_3(M20) and FeF_3(M50), PTFE: $Fe(C_2O_4)\cdot 2H_2O$: melamine (2: 1: 0.2 and 2: 1: 0.5 wt ratio) were used. In all cases the mixture was dried on a hot plate, then ground and molded into pellets, which were then fired at 600 °C with ramping rate of 200 °C/h for 1 h under Ar in a covered alumina crucible.

Material characterization

X-ray diffraction (XRD) patterns of the samples were obtained with a Rigaku using Cu Kα radiation in the 2θ range from 20° to 70° at a rate of 3°/min. The XRD patterns were analyzed using MDI jade 6 software program and refined using X’pert Highscore plus(The reference ICSD number of ReO_3-type FeF_3 phase is #16671 and of tetragonal FeF_2 phase is #65702). The amounts of carbon and nitrogen (N) in the samples were measured using a Vario EL III (Analysensysteme, GMBH). Morphologies of the samples were observed using a scanning electron microscope (SEM, XL30S, Philips Electron Optics B.V.). Morphology of the FeF_3(R) sample was observed using a transmission electron microscope (TEM, JEM-2100F, JEOL). Morphology and electron energy loss spectroscopy (EELS) maps of FeF_3(M20) were obtained using a HR-[S]TEM(JEM-2200FS, JEOL).

Electrochemical properties

Electrodes were fabricated by manually mixing the resulting material and carbon (Super-P, Timcal) with PTFE binder in a ratio of 70: 25: 5 (wt%). Electrodes were punched with diameter of 8 mm. Electrochemical properties were measured using Swagelok-type cell. Cells were assembled with the composite electrode, separator (Celgard 2400), electrolyte ($LiPF_6$ in EC/DEC, 1:1), and Li metal as a negative electrode. All cells were assembled in an Ar-filled glove box. All electrochemical tests were performed at room temperature.

Galvanostatic Intermittent Titration Technique (GITT) measurement were performed to characterize Open-Circuit Voltage (OCV) and polarization at each lithiation state of the FeF_3(R), FeF_3(M20) and FeF_3(M50) samples after one cycle with current rate of 10 mA/g. The applied current density in GITT measurement was 5 mA/g (~ 0.021C) for an intermittent step of 1 h and for 3 h rest. GITT conditions were all the same in the three samples. All cell tests were followed by the first activation cycling with current rate of 10 mA/g at discharge and charge.

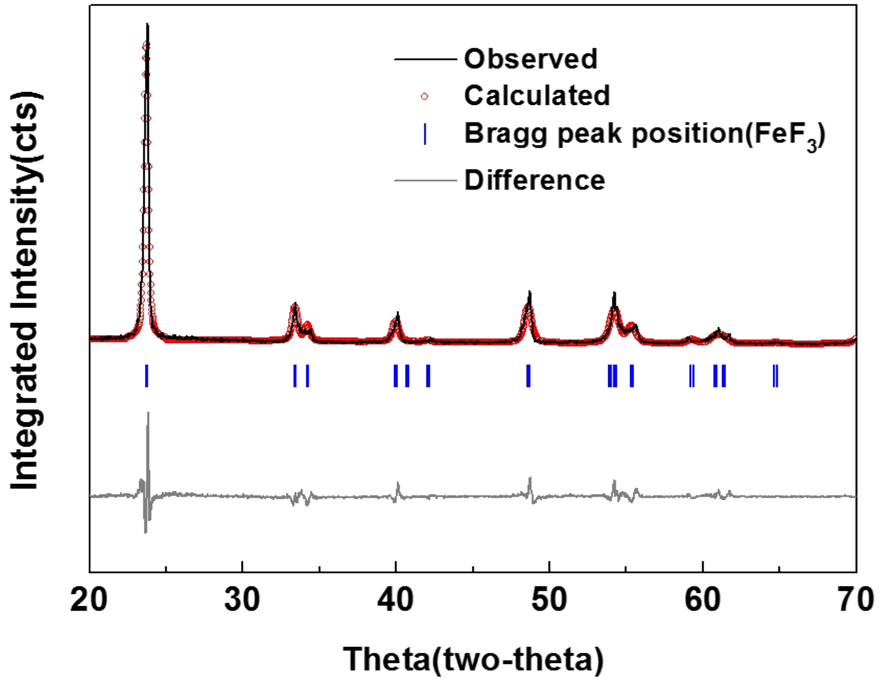

Figure S1 Rietveld refinement of XRD patterns of FeF_3(M50)

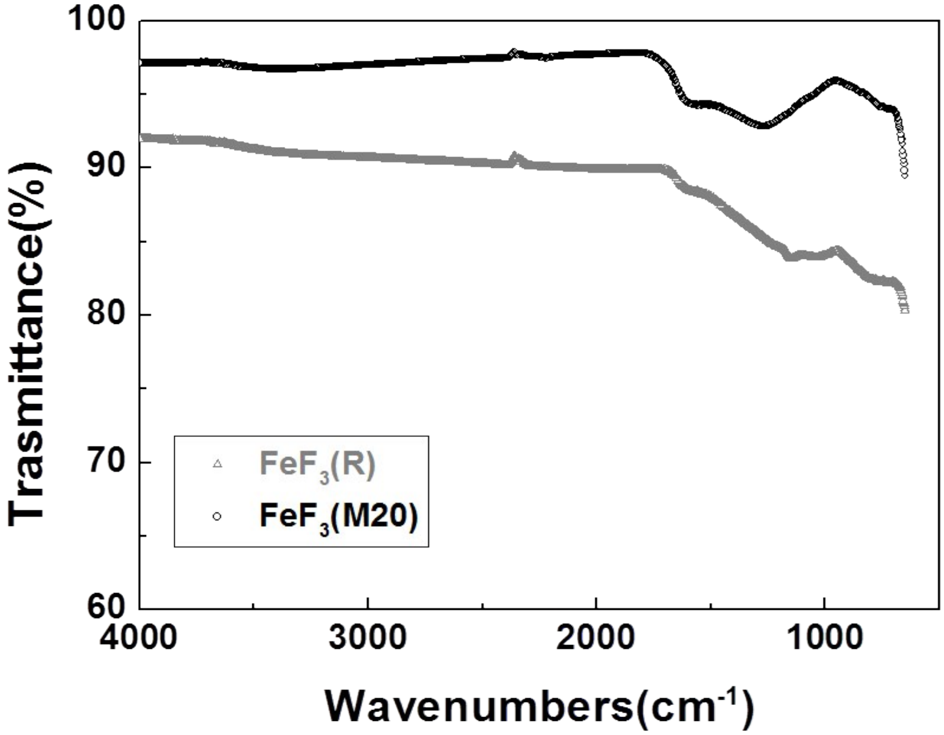

Figure S2. FT-IR spectra of FeF_3(R) and FeF_3(M20) measured in ATR (Attenuated Total Reflection) mode.

Fourier Transform-Infrared Spectroscopy (FT-IR) spectra of FeF_3(R) and FeF_3(M20) were measured in powder form for identifying the existence of hydrated FeF_3 in the two samples. In case of $FeF_3 \cdot 3H_2O$, a strong and broad absorption band in the region 2850 - 3450 cm^{-1} which is originated from the hydrogen bond associated with crystal water was attributed to –OH stretching vibration and the absorptions at 1639cm^{-1}, 710cm^{-1} and 790cm^{-1} were from H-O-H in-plane and out-plane bending vibration.[2] Both FeF_3(R) and FeF_3(M20) did not show specific absorption peaks in the region of 2850 – 3450 cm^{-1}. This indicates that the two samples were anhydrous form even though the samples were treated in air atmosphere.

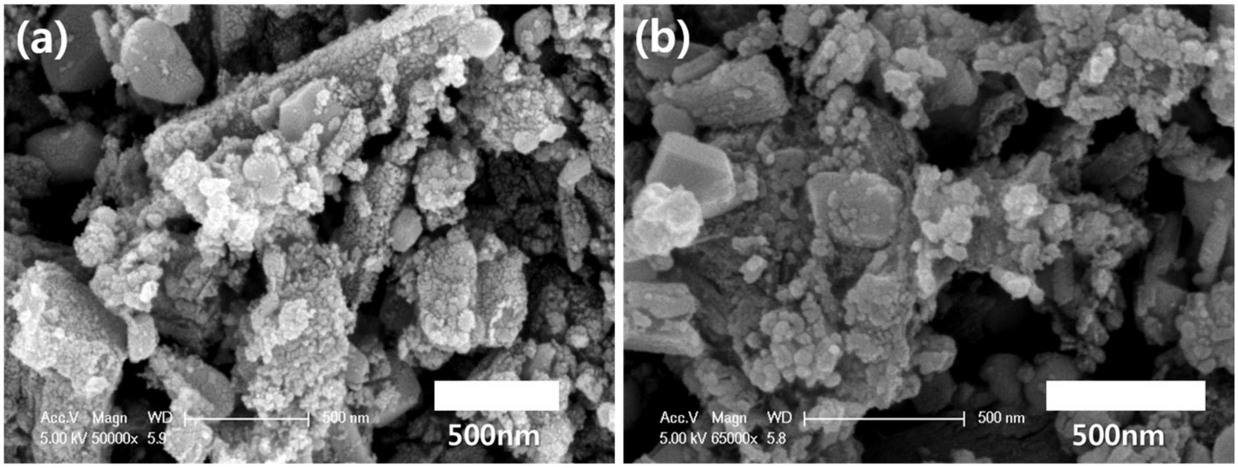

Figure S3 SEM images of (a) FeF_3(R), (b) FeF_3(M20)

SEM images of FeF_3(R) (Figure S3a) and FeF_3(M20) (Figure S3b) show that both have particles of sizes 20nm ~ 200nm.

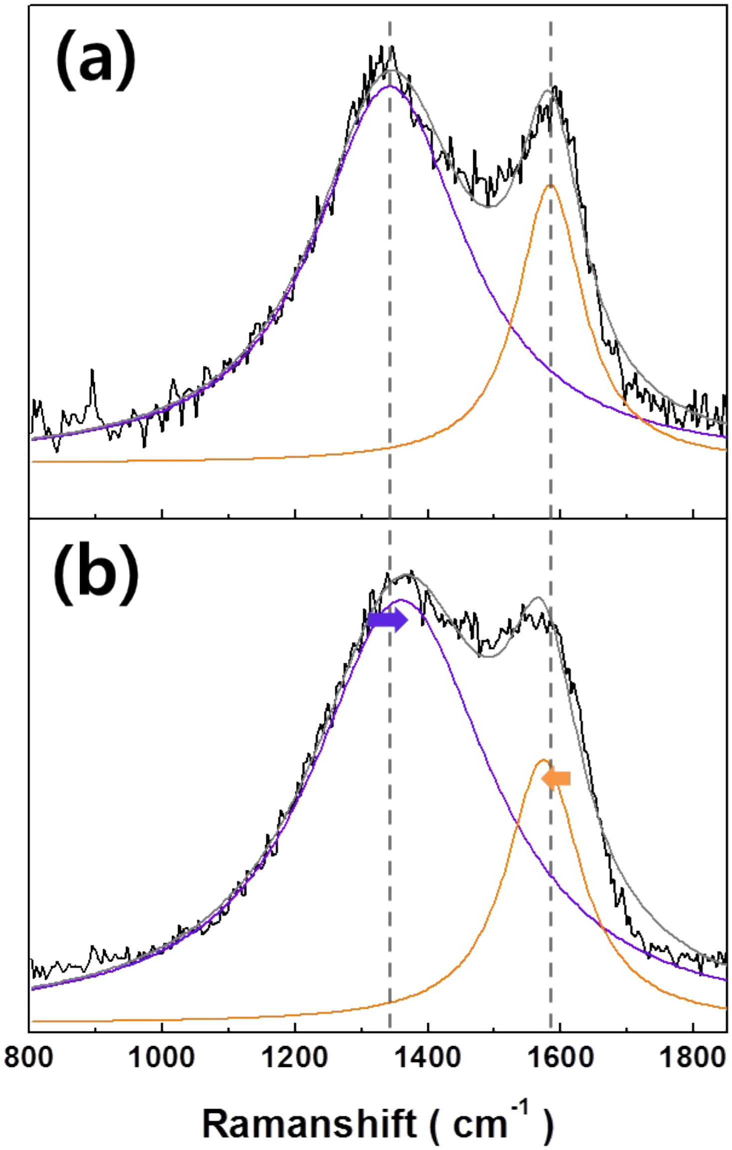

Figure S4. Raman spectra of (a) the FeF_3(R) sample and (b) the FeF_3(M20) sample

Figure S4 shows Raman spectra of FeF_3(M20) and FeF_3(R). Both samples show two characteristic bands of carbon spectra. The G band is a characteristic of graphitic layers while the D band is a characteristic of disordered carbon or defective graphitic structures. By using Lorentzian curve-fitting, D band in FeF_3(R) was around 1342 cm^{-1} and G band was around 1584 cm^{-1} and was overlapped with G band. Furthermore, the intensity ratio of D band/G band (I_D/I_G)

in FeF_3(R) is 1.35. Compared to FeF_3(R), G band in FeF_3(M20) has more overlapped with D band and Raman spectra of FeF_3(M20) is fitted in two features, with D band around 1359cm^{-1} and G band around 1573cm^{-1}. Also, I_D/I_G band intensity ratio in FeF_3(M20) is 1.60 and higher than that in the FeF_3(R) sample. This high band intensity ratio indicates that the incorporation of N can generate large amount of defects into the structure of amorphous carbon in the FeF_3(M20) by using melamine.[3] These features of Raman spectra suggest that nitrogen can be incorporated into amorphous carbon in FeF_3(M20).

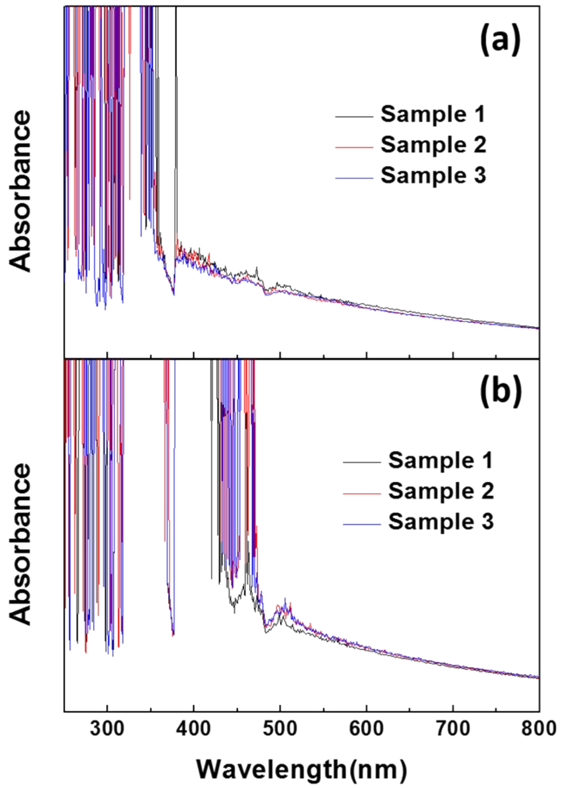

Figure S5 UV vis absorption spectra of FeF_3(R)_(a) and FeF_3(M20)_(b)

UV vis absorption spectra of FeF_3(R) and FeF_3(M20) were observed in the integration mode using pellet based on KBr carrying out with 1wt% of each samples. Optical absorption behavior shows at ~350nm for FeF_3(R) whereas that of FeF_3(M20) shows at ~450nm. The higher absorption wavelength in FeF_3(M20) sample than FeF_3(R) directly indicates that the bulk FeF_3 phase in FeF_3(M20) has narrower band-gap than that of FeF_3(R). Though the large content of each samples strongly scattered light source forming noisy spectra, it is remarkable that N-doped composite shows clearly different optical absorption behavior than bare composite meaning electronic property in the FeF_3(M20) can be originated from the incorporation of nitrogen into bulk.

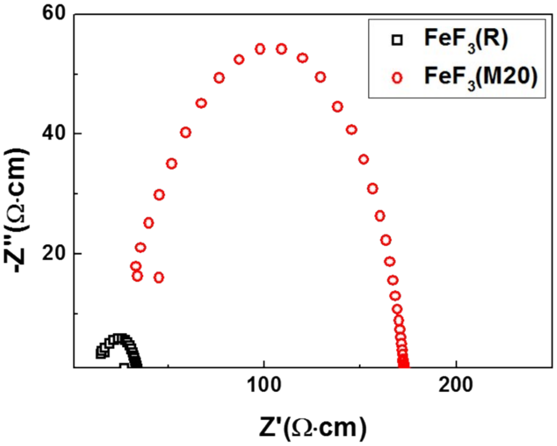

Figure S6 Impedance spectra of the FeF_3(R) powder and the FeF_3(M20) powder

The two samples have large amount of carbon, ~17 wt% in the composite. The composite electronic conductivity of the two samples will be very high due to large amount of carbon and then the result will be from the percolation of electron in the composites rather than the bulk electronic conductivity.

However we've measured EIS as shown in Figure S6. The composite electronic conductivity of FeF_3(R) and FeF_3(M20) was evaluate with Swagelok-type cell where the powder sample put into the cell with pressure. The composite electronic conductivity of each powder sample are 2.83*10-1 S/cm for FeF_3(R) and 5.74*10^{-2} S/cm for FeF_3(M20) and the high electronic conductivities of both samples, ~10^{-2} S/cm, are mainly due to large amount of carbon as expected. However, the incorporated nitrogen in the carbon of FeF_3(M20) does not improve the electronic conductivity of the composite because nitrogen bonding configuration to carbon in FeF_3(M20) is pyrrolic N and pyridinic N as shown in Raman spectroscopy in Figure S4, not graphitic N that can improve electronic conductivity.

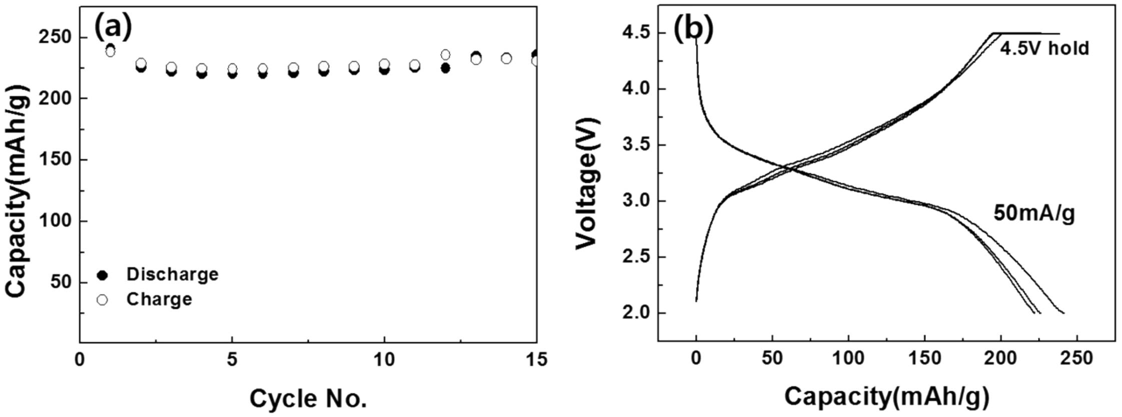

Figure S7 (a) FeF_3(M20) capacity retention at low current rate of 50 mA/g with a voltage hold at 4.5 V for I < 5mA/g, and (b) voltage profiles of first 3 cycles with low current rate of 50 mA/g at a voltage range of 2.0 – 4.5V.

FeF_3(M20) electrode achieved 225mAh/g of capacity, 95% of theoretical capacity, at low current rate for 15 cycles without significant fading.

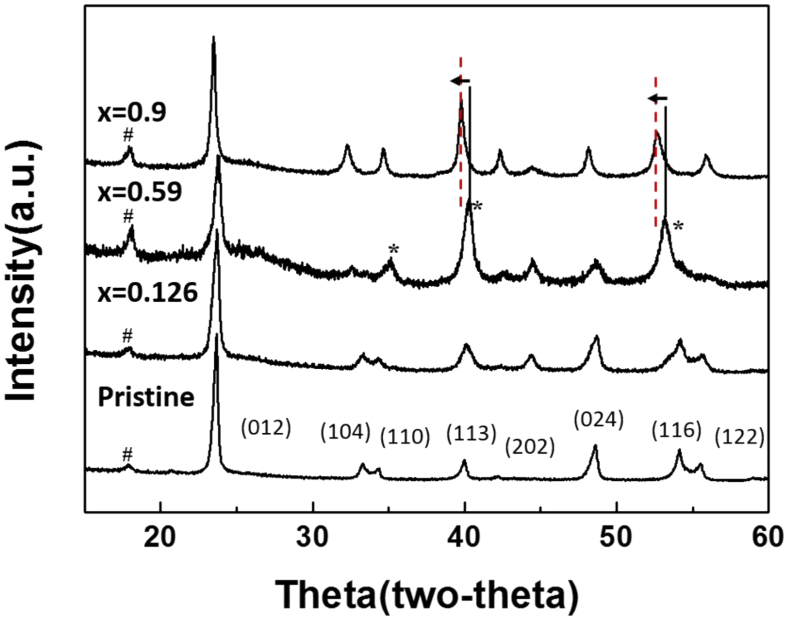

Figure S8. Ex-situ XRD patterns of FeF_3(M20) electrode during 1st discharge at each lithiated amount, x in Li_xFeF_3. Stars (*) indicate new peaks and '#' is from PTFE (Binder). All electrodes were discharged at current rate of 10 mA/g and DMC washed after cell test; terminating condition for each electrode were cut-off voltage with 3.28V for x = 0.126, 3.0V for x = 0.59 and 2.0V for x = 0.9. The peak at 18° denotes PTFE which is a binder composing the electrodes.

The lithium insertion into FeF_3(M20) was investigated by *ex-situ* XRD in Figure S8. From x = 0.126 to x = 0.59, several new peaks as shown in star (*) in Figure S8 are appeared. This new peak appearance indicates that 2nd phase is formed as a lithiation progresses. In lithiation region of x = 0.59 to x = 0.9, there are the shifts of XRD peaks toward the low two-theta angle. This peak shift without forming new peaks means the increase of lattice parameter. This also indicates that the lithiation reaction occurs with a solid-solution reaction process. These structural changes in FeF_3(M20) were quite similar to the reported structural changes of FeF_3 in the literature.[4]

Therefore, the improved electrochemical activity in FeF_3(M20) may not be from the structural changes.

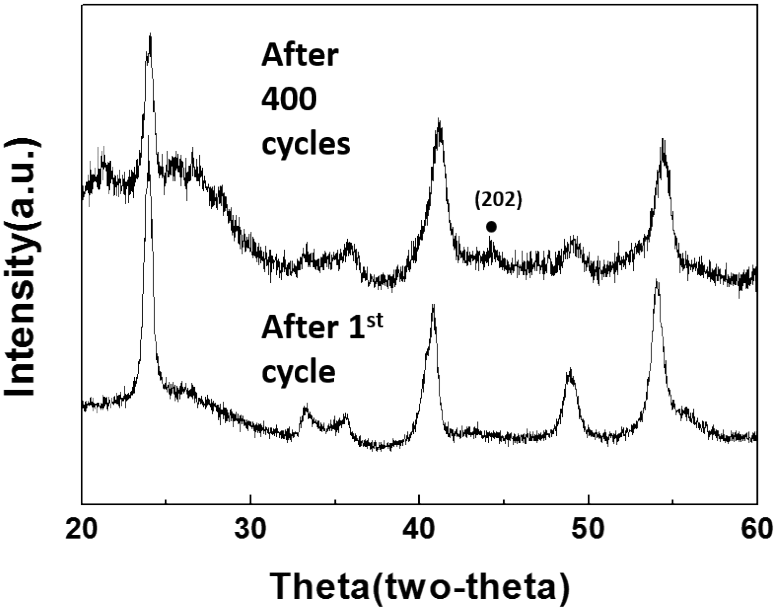

Figure S9**.** Ex-situ XRD patterns of FeF_3(M20) electrode after 1st cycle at current rate of 10 mA/g and after 400 cycles at 4C charge /16C discharge. The hump between 20° - 30° in 400 cycled electrode is from polymer separator which was still attached. The (202) peak denoted by '•' at ~ 44° after 400 cycles was from unreacted FeF_3 due to lack of electrochemical activity at high rates

To understand structural stability of FeF_3(M20) during cycles, ex-situ XRD of the electrode after 1st cycle in current rate of 10 mA/g and the electrode discharged at 4000 mA/g for 400 cycles were carried out. Figure S9 clearly shows that FeF_3 structure after 400 cycles at high rates was barely changed. Furthermore, the crystalline structure of FeF_3(M20) was well maintained even after 400 cycles compared to that after 1st cycle. As the operating voltage region was from 2.0V to 4.5V which only allows reversible intercalation reaction of FeF_3, the structural change barely happens without the collapse of the structure.

Table 1 Refined lattice parameters and elemental analysis data of FeF_3(R), FeF_3(M20) and FeF_3(M50)

Sample	Lattice parameter [Å]		Element [wt%]	
	a	c	N	C
FeF_3(R)	5.212(7)	13.308(4)	0.045	16.76
FeF_3(M20)	5.227(9)	13.267(0)	6.332	16.77
FeF_3(M50)	5.229(8)	13.267(5)	12.102	18.90

Reference

1. J. Lee and B. Kang, *Chemical communications*, 2016, DOI: 10.1039/C6CC03706B.
2. C. Chen, X. Xu, S. Chen, B. Zheng, M. Shui, L. Xu, W. Zheng, J. Shu, L. Cheng, L. Feng and Y. Ren, *Materials Research Bulletin*, 2015, **64**, 187-193.
3. Q.-H. Yang, P.-X. Hou, M. Unno, S. Yamauchi, R. Saito and T. Kyotani, *Nano Letters*, 2005, **5**, 2465-2469.
4. F. Badway, N. Pereira, F. Cosandey and G. G. Amatucci, *Journal of The Electrochemical Society*, 2003, **150**, A1209.